Research Square

Preprints are preliminary reports that have not undergone peer review.
They should not be considered conclusive, used to inform clinical practice,
or referenced by the media as validated information.

Mechanistic Study of Tetracycline Removal and Degradation in Water Using nCo@nZVI Composite Materials within a Fenton System

Shuxian WEI
Anhui University of Technology
Lanyue ZHANG
Anhui University of Technology
Gang DU
Anhui University of Technology
Canhua LI
licanhua1979@163.com

Anhui University of Technology
Chuan HE
Jiuquan Vocationl and Technical College
Minghui LI
Anhui University of Technology
Jiamao LI
Anhui University of Technology
Aiqin MAO
Anhui University of Technology
Yanran WANG
Anhui University of Technology

Research Article

Keywords: Nano zero valent iron, Nano cobalt, Bimetallic, Fenton system, tetracycline

Posted Date: November 13th, 2024

DOI: https://doi.org/10.21203/rs.3.rs-5364501/v1

License: This work is licensed under a Creative Commons Attribution 4.0 International License.
Read Full License

Additional Declarations: No competing interests reported.

Abstract

In response to the increasingly severe antibiotic pollution in water bodies, this study developed a new type of magnetic nano cobalt @ nano zero valent iron that is easy to prepare and inexpensive(nCo@nZVI) Composite materials. The magnetic sheet-like nZVI was prepared using a rheological phase inversion method, followed by the synthesis of nCo@nZVI through liquid-phase reduction. The material's physical and chemical properties, along with its structure, were meticulously characterized through the utilization of various techniques, including BET, FESEM, XRD, HRTEM, EDS, XPS, and FTIR. Batch experiments were conducted to evaluate the adsorption-degradation mechanism of TC by the material in the Fenton system, and to investigate the effects of factors such as temperature, pH value, and initial TC ion concentration on removal efficiency. The results indicated that under conditions of pH 7 and temperature of 20°C, the nCo@nZVI material could reduce the TC concentration in wastewater from an initial 20mg/L to trace levels within 120 minutes. Adsorption kinetics and isotherm analysis revealed that the adsorption process of TC by nCo@nZVI followed a pseudo-second-order kinetic model and Langmuir isotherm model, indicating predominantly chemical adsorption with an adsorption capacity of 25.33mg/g. Thermodynamic studies have shown that the adsorption of TC by nCo@nZVI occurs spontaneously. Furthermore, the nCo@nZVI composite material is environmentally friendly and cost-effective. It has the advantages of being recyclable and reusable under external magnetic fields, showing great potential in the remediation of antibiotic contaminated sites, and this method has guiding significance for the recovery of cobalt containing wastewater.

1. Introduction

Emerging contaminants, including pharmaceuticals and personal care products (PPCPs), are increasingly being detected in the natural environment. These contaminants are challenging to degrade and often exhibit a "pseudo-persistent" state in water bodies, posing significant threats to ecosystems and human health[1]. Antibiotics, being among the most widely used drugs in healthcare, experienced a dramatic rise in global consumption during the COVID-19 pandemic[2]. Once these antibiotics enter living organisms, approximately 30–90% are excreted into the environment, further exacerbating environmental and health risks[3]. Tetracycline antibiotics, in particular, are relatively stable in acidic conditions and resistant to oxidation in the environment, but they become unstable under extreme pH conditions, leading to low volatility and poor degradation of byproducts[4]. Therefore, effectively remediating antibiotic-contaminated water and soil while ensuring the safety of crops and human health has become an urgent and critical challenge. Developing cost-effective methods to prevent the infiltration of tetracycline residues into everyday life is now more necessary than ever[5].

In the treatment of tetracycline antibiotics, commonly used methods include adsorption[6], biodegradation[7], and advanced oxidation processes (AOPs) [8]. Among these, chemical methods are employed to treat pollutants by applying chemical principles, with techniques such as photocatalysis, Fenton oxidation, ozone oxidation, and chemical coagulation commonly used to remove antibiotics from

water. Fenton oxidation, in particular, often works synergistically with other AOPs[9]. AOPs generate highly reactive free radicals, such as hydroxyl radicals (•OH) and sulfate radicals ($\mathbf{SO}_4^-$•), via the utilization of light radiation, electric current, high temperature and pressure, or the presence of catalysts. These free radicals react with persistent pollutants, ultimately breaking them down into low-toxicity or non-toxic small molecules[10, 11]. Compared to other advanced oxidation processes, AOPs are particularly favored for their simplicity, rapid reaction rates, and ability to produce flocculation.

In recent years, engineered magnetic nanoparticles have been extensively applied in the fields of wastewater treatment and environmental remediation. The synthesis of nanoscale zero-valent iron (nZVI) encompasses a variety of methods, including chemical reduction using sodium borohydride ($NaBH_4$) as the reductant, electrochemical reduction, carbothermal reduction, green synthesis, and ultrasound-assisted synthesis. However, these methods often encounter challenges such as high raw material costs, toxic or explosive by-products, hazardous operating procedures, and high energy consumption[12, 13]. Therefore, the primary goal in developing new nZVI production methods is to reduce production costs and facilitate the broader application of nZVI in practical settings. Similarly, in the field of nanomaterials, cobalt-iron alloys, like nZVI, have shown significant potential across various domains due to their unique physical and chemical properties, despite the challenges they face[14].

Cobalt-iron alloys possess unique soft magnetic properties, including high saturation magnetization, high Curie temperature, low coercivity, high magnetic permeability, and low magnetocrystalline anisotropy constant. As a critical magnetic nanomaterial, cobalt-iron alloys have been widely utilized in strategic fields such as aerospace generators, computer read-write heads, micro-electromechanical systems (MEMS), magnetic keys, and the automotive industry[15, 16]. Due to quantum size effects, these materials also show great potential in applications related to magnetism, catalysis, and electromagnetic wave absorption[17, 18]. Yang et al.[19] investigated the adsorption of nitrate nitrogen in water using cobalt-iron layered bimetallic biochar. Their results showed that the material has a significant adsorption capacity for nitrate nitrogen, with an adsorption rate of 88.52 mg/g. The adsorption kinetics followed a pseudo-second-order kinetic model, and the isotherm data aligned with the Langmuir isotherm model. The adsorption mechanism involved ion exchange, ligand exchange, electrostatic attraction, and hydrogen bonding. This material exhibited strong affinity for nitrate nitrogen in water bodies containing various coexisting anions, highlighting its potential for practical applications.Ming et al. [20]developed cobalt-iron nitride/alloy nanosheets (CoFe-NA/NF) on foam nickel using a simple three-step method. These nanosheets acted as bifunctional catalysts for both the hydrogen evolution reaction (HER) and oxygen evolution reaction (OER), offering a novel approach to designing bifunctional catalysts for overall water splitting. Additionally, Xie et al. [21] created carbon nanofibers (Fe/Co-CNFs) with a rough surface and uniformly distributed iron/cobalt alloy nanoparticles. Their research demonstrated that Fe/Co-CNFs have a large specific surface area and numerous active sites, enabling the complete electrocatalytic degradation of tetracycline into CO₂ and water. This finding provides a new material for the environmental remediation of water bodies contaminated with antibiotics.

This study investigates an economical and facile approach for the removal of tetracycline from aqueous solutions using rod-shaped nCo@nZVI composite materials. In this work, FeCl·4H O served as the primary precursor, while sodium hydrosulfite($Na_2S_2O_2$), an inexpensive reducing agent, was utilized to synthesize magnetic sheet-like nZVI materials via a rheological phase reaction. These materials were subsequently reduced to produce the nCo@nZVI composite. Comprehensive characterization of the material's physicochemical properties and microstructure was conducted using a range of techniques, including FESEM, EDS, HRTEM, XRD, XPS, BET, and FTIR. The study further explored the influence of tetracycline concentration, temperature, and pH on the removal efficiency of tetracycline. The findings suggest that nCo@nZVI nanomaterials demonstrate a remarkable efficiency in eliminating tetracycline ions from water. Additionally, the adsorption characteristics of the nCo@nZVI composite towards tetracycline, as well as the adsorption and degradation mechanisms within a Fenton system, were examined in detail. The objective was to identify a cost-effective and efficient method for the treatment of tetracycline-contaminated wastewater. This research not only addresses the pressing issue of tetracycline pollution and the reutilization of agricultural waste resources but also provides significant insights with potential applications in environmental pollution mitigation.

2. Experimental

2.1. Chemicals and regents

Tetrahydrate ferrous chloride ($FeCl_2·4H_2O$), sodium chloride (NaCl), cobalt chloride ($CoCl_2$), hydrochloric acid (HCl), tetracycline ($C_{22}H_{24}N_2O_8$), sodium hydroxide (NaOH), high-purity nitrogen gas (99% purity) sodium hydrosulfite ($Na_2S_2O_2$). All chemicals used are analytical grade, purchased from Shanghai McLean Biochemical Technology Co., Ltd., and prepared into the required solution using deionized water.

2.2 Experimental Methods

2.2.1 Preparation nCo@nZVI Nanomaterial methods

The first step is the preparation of nZVI material. Thoroughly mix NaOH and $Na_2S_2O_2$ in a 1:1 mass ratio to obtain a solid mixture. During the mixing process, avoid contact with moisture and control the humidity and temperature in the glove box to prevent sodium hydroxide from absorbing water. Transfer the mixture to a beaker, seal it for storage, and place it in a nitrogen-rich glove box for later use.

The experiment for preparing nZVI material was conducted in a glove box under N_2 protection. During all processes involving $FeCl_2·4H_2O$, strict anaerobic conditions must be maintained to prevent the oxidation of Fe(II) to Fe(III). Weigh an appropriate amount of $FeCl_2·4H_2O$ in the glove box and thoroughly mix it with the solid mixture in the beaker. The mixed reactants were placed in an ice bath, and an appropriate amount of deionized water was slowly added using a spray bottle while stirring was intensified until the reactants entered the rheological phase and the chemical reaction commenced. After maintaining continuous stirring for a certain period, stirring was ceased and the reactants were allowed to cool

naturally to room temperature. Following the completion of the reaction, the cooled reaction product was filtered under a nitrogen atmosphere and washed repeatedly with oxygen-free distilled water and anhydrous ethanol to isolate the prepared nZVI particles. Subsequently, the supernatant was removed by centrifugation, and ultrasonic cleaning was performed until the solution reached a neutral pH. Finally, the nZVI material was obtained after vacuum drying.

Step 2: Synthesis of nCo@nZVI nanometer material. First, add 100 mL of deionized water to a three-necked flask and allow nitrogen to flow for 30 minutes. Next, add a specific amount of hexahydrate cobalt chloride ($CoCl_2 \cdot 6H_2O$) and stir mechanically for 10 minutes to ensure full dissolution. Then, add 100 mg of elemental nZVI, synthesized according to the first step, to the mixed solution. Gradually heat the mixture to 55°C and maintain this temperature for 2 hours to ensure that the cobalt salt is fully reduced by the nZVI. The entire process should be carried out under nitrogen protection with continuous mechanical stirring. Finally, collect the precipitate by centrifugation and wash it several times with deionized water and ethanol, respectively. The washed material was placed in a vacuum drying oven and subjected to drying for 24 hours to obtain the nCo@nZVI nanomaterial. The detailed synthesis process flowchart for nCo@nZVI nanomaterials is shown in Fig. 1.

2.2.2 Experimental method for tetracycline removal

First, dissolve a specific amount of tetracycline (TC) in deionized water to prepare an original solution with a concentration of 100 mg/L. Gradually dilute this stock solution according to the experimental conditions. Transfer 100 mL of the diluted solution into a 250 mL Erlenmeyer flask. Place the flask in a constant temperature shaker set to 20°C and a speed of 200 rpm, then add a specified amount of nCo@nZVI nanometer material. At regular intervals, withdraw samples, filter them through a 0.22 μm filter membrane, and analyze the concentration using a UV-visible spectrophotometer. Perform two parallel experiments to account for potential errors. The removal amount (Qt) and removal rate (η) of TC by the materials are calculated using the following formulas:

$$\varvec{Q}_{\varvec{t}} = (\varvec{C}_0 - \varvec{C}_{\varvec{t}}) \times \varvec{V}/\varvec{m}$$

4

$$\varvec{\eta} = (\varvec{C}_0 - \varvec{C}_{\varvec{t}})/\varvec{C}_0 \times 100\%$$

5

In the equation, $\varvec{C}_0$ represents the initial concentration (mg/mL) of TC at time t = 0, $\varvec{C}_{\varvec{t}}$ represents the concentration (mg/mL) of TC at time t, V represents the volume (L) of the solution, and m represents the amount (mg) of the material added.

2.2.3 TC detection method

This article employs a UV-visible spectrophotometer to determine the concentration of tetracycline (TC) in the filtrate. Prepare TC solutions with concentrations of 0 ~ 20 mg/L. Transfer 3 mL of each solution into small brown bottles. Using water as a reference, measure the absorbance (A) at a wavelength of 357 nm with the UV-visible spectrophotometer. The standard curve for TC is shown in Fig. 2(a), with the equation y = 0.29367x-0.03171 and R^2 = 0.9935, where y represents absorbance and x denotes the initial concentration. The concentration of TC in the samples can be determined from this standard curve.

3. Results and discussion

3.1 Characterization of Materials

3.1.1 XRD, HRTEM, and FESEM characterization analysis

Figure 2 (b) shows nCo@nZVI XRD patterns of nanomaterials. As illustrated in the figure, the diffraction peaks of 2θ at 44.67 °, 65.02°, and 82.33° correspond to α-Fe [22]. In addition, diffraction peaks of $CoFe_2O_4$ appeared at 2θ of 18.31°, 30.55°, 35.86°, 43.76°, and 62.15°. This indicates that the main reaction products of the experiment are $CoFe_2O_4$ and α-Fe [23].

The morphological characteristics of nCo@nZVI nanocomposites were observed using field emission scanning electron microscopy (FESEM). Figure 3(a) shows that nZVI particles form a sheet-like structure with significantly reduced aggregation, while $CoFe_2O_4$exhibits a radial morphology. Upon further magnification, the nCo@nZVI nanocomposite materials display distinct rod-like structures, with lengths ranging from 100 to 2000 nanometers and thicknesses less than 100 nanometers. Figures 3(c-f) present the energy dispersive spectroscopy (EDS) results of the boxed area in Fig. 1. Additionally, the transmission electron microscopy (TEM) line scan images of the nanosheets in Figs. 3(k) and 3(l) reveal that the main elements of the nanosheets are Fe, Co, S, and O. SEM testing at different magnifications confirmed the material's morphology, uniformity, microstructure, and particle size. The results indicate that the nanorods have a solid structure, smooth surface, and uniform size, exhibiting the characteristics of hexagonal prism-shaped nanorods [24].

Further observation using high-resolution transmission electron microscopy (HRTEM) is shown in Fig. 3(h), where TEM images of some nanosheets reveal dark mottled structures within a single nanosheet. Figures 3(l) and 3(i) provide detailed views of the crystal structure in these bright and dark regions. At higher resolution, the lattice spacing in the dark regions is 0.20267 nm, corresponding to the body-centered cubic (110) plane of α-Fe. The interplanar spacing in the light-colored regions is 0.25310 nm and 0.2099 nm, corresponding to the (311) and (400) crystal planes of the $CoFe_2O_4$ phase, respectively. These measurements are consistent with the results from XRD analysis. Additionally, the selected area electron diffraction (SAED) image of the material in Fig. 3(i) shows distinct continuous diffraction rings corresponding to the (311), (222), and (440) crystal planes, further aligning with the XRD analysis results [25]. From this, it is evident that the reaction product is a composite nanosheet

composed of sheet-like α-Fe and rod-shaped $CoFe_2O_4$, which can be referred to as nCo@nZVI nanocomposite materials.

3.1.2 BET and FTIR characterization analysis

The adsorption performance of nCo@nZVI nanomaterials is significantly governed by their specific surface area and pore size distribution characteristics. To this end, the present study employed N_2 adsorption-desorption analysis to characterize the specific surface area and pore structure of nCo@nZVI nanomaterials. As depicted in Fig. 4(a), the material exhibits a typical Type IV isotherm, revealing its mesoporous lamellar structure, which encompasses narrow slit-like pores along with some hollow and microporous regions. A pronounced hysteresis loop is observed within the P/P_0 range of 0.6 to 1.0, attributed to capillary condensation, further confirming the typical characteristics of a Type IV isotherm [26]. Moreover, the nCo@nZVI nanomaterial demonstrates a high specific surface area of 42.0122 m²/g.

Figure 3(b) displays the FTIR spectroscopy analysis results of nCo@nZVI nanomaterials. In the spectrum, the absorption peaks at 1630 cm⁻¹ and 3400 cm⁻¹ correspond to the bending vibration mode of water molecules H-O-H and the stretching vibration of surface hydroxyl groups (-OH), respectively [27], indicating the occurrence of hydroxylation on the surface of nCo@nZVI. According to reports in literature [28, 29], metal oxide surfaces are covered with hydroxyl groups, which exhibit different forms as the pH value changes. Therefore, the surface charge state of nCo@nZVI nanomaterials in aqueous solution will fluctuate with pH values. Additionally, the peak to the right of 500 cm⁻¹ in the spectrum is associated with the stretching vibration of Fe-S within the nCo@nZVI nanomaterial[30, 31]. During the synthesis process of the material, these functional groups can effectively capture Fe(II) from the solution, facilitating the loading of nanoscale zerovalent iron.

3.1.3 X-ray Photoelectron Spectroscopy (XPS) characterization analysis

XPS was utilized for qualitative analysis of the elemental composition based on the characteristic spectral lines observed in the energy spectrum of nCo@nZVI. Figure 4(c) presents the XPS survey spectrum of the nCo@nZVI nanomaterials, with binding energy peaks corresponding to S 2p, O 1s, Fe 2p, and Co 2p, respectively, from low to high energies, further confirming the coexistence of iron and cobalt in these nanomaterials. In Fig. 4(d), the characteristic peaks at 708.9 eV and 719.7 eV are attributed to Fe(0), while those at 710.1 eV and 724.5 eV represent Fe(II), indicating that Fe(II) and Fe(0) are the primary iron species in the nanomaterials. On the surface of the core-shell structure, iron primarily exists in the forms of Fe(II) and Fe(III), whereas in the core region [32], it is mainly present as Fe(II) and Fe(0). Based on these observations, it is hypothesized that the nCo@nZVI nanomaterials may possess a core@shell structural feature with Fe(0) concentrated in the core region [33]. This finding aligns with previous research indicating that the outer oxide layer of nZVI is primarily composed of FeOOH、FeO、α/γ-Fe_2O_3, and Fe_3O_4[34]. Consistent with the conclusions of other researchers, the present study also points

out that the oxide surface of nZVI is composed of specific components. Specifically, Fe 2p spin-orbit split peaks were observed at energies of 706.8 eV and 723.5 eV, attributed to the photoelectron contributions of Fe(III), Fe(II), and Fe(0). During Ar^+ sputtering, although the signal of Fe(0) increased slightly, the magnitude of this enhancement was modest, suggesting that α-Fe is not widely dispersed or precipitated within the Fe_3O_4 matrix.

In Fig. 4(e), the distinct spectral peak at Co 2p3/2 (781.2 eV) corresponds to Co(II), indicating that cobalt exists in the form of CoO or Co(OH)₂ in the nCo@nZVI nanomaterials [35]. The peak at 786.8 eV is identified as the satellite peak of Co(II) [36]. Additionally, in cobalt iron hydroxide, the Co 2p1/2 peak (796.6 eV) shifts towards lower energy, suggesting that the dominant layer formed on the surface of the nCo@nZVI nanomaterials may enhance their reactivity. Furthermore, during the synthesis process, some sulfur is oxidized to form sulfur oxides. In summary, the surface shell of nCo@nZVI nanocomposites is primarily composed of sulfur oxides with a small amount of iron (hydrogen) oxides.

Figure 3(f) shows the O 1s peak splitting results for nCo@nZVI nanomaterials. In the fine spectrum, the peaks at 530.18 eV, 532.47 eV, and 533.60 eV correspond to lattice oxygen (Fe-O, Co-O), chemisorbed oxygen, and surface-adsorbed oxygen, respectively. The presence of lattice oxygen confirms the formation of metal oxides following carbonization treatment. Chemisorbed oxygen refers mainly to O_2 or $\mathbf{O}_2^{2-}$ adsorbed on the surface of metal oxides, which have high activity and a fast migration rate, aiding in the acceleration of the material's electron transfer process [37]. Surface-adsorbed oxygen mainly includes oxygen vacancies on the material's surface, as well as oxygen or oxygen-containing substances (such as H₂O), whose presence can influence the material's catalytic performance [38].

3.2 Effects of Initial TC Concentration

At pH 7 and a temperature of 20°C, the effect of different initial concentrations of tetracycline (TC) on the removal efficiency was studied using nCo@nZVI nanomaterials at a dosage of 1 g/L. The experimental results indicate that when the initial concentration of TC is low, nCo@nZVI nanomaterials effectively remove TC from wastewater. Especially when treating simulated wastewater samples with an initial TC concentration of 20 mg/L, the nCo@nZVI nanomaterials were able to effectively reduce the TC concentration to trace levels within approximately 120 minutes, achieving a removal efficiency close to 100%. This outcome suggests that under the specified conditions, the nanomaterials offered abundant active sites for TC molecules to occupy. However, as the initial TC concentration increased to 50 mg/L, the removal efficiency gradually declined to 48.67% [39]. This may be attributed to the limited number of binding sites on the surface of the nCo@nZVI nanomaterials, which constrained the effective adsorption and removal of TC molecules from the solution, thereby resulting in a decrease in removal efficiency. In view of this, for high-concentration wastewater treatment scenarios, considering an increase in the dosage of nCo@nZVI nanomaterials or the introduction of other treatment methods may become effective strategies to enhance removal efficiency.

The experimental results also showed that nCo@nZVI nanomaterials can efficiently remove TC from aqueous solutions, with the four control groups with different initial concentrations almost reaching equilibrium simultaneously at around 120 min. This indicates that nCo@nZVI nanomaterials have a strong ability to remove TC. When removing low-concentration simulated wastewater, nCo@nZVI nanomaterials exhibit extremely high processing efficiency, overcoming the challenges faced by traditional methods such as adsorption, membrane separation techniques, ozone oxidation, and photocatalytic oxidation in removing low-concentration TC [40].

3.3 The influence of initial pH value.

Due to the multiple ionizing functional groups of tetracycline, the pH value of the solution significantly affects the number of charges carried by its molecules and their forms of existence. The pH value of the solution has a significant impact on the removal of TC. Tetracycline molecules are multifunctional amphiphilic molecules, and their surface charge is closely related to the pH value of the solution: when pH > 7.7, tetracycline molecules carry a negative charge; when 3.3 < pH < 7.7, tetracycline molecules carry both negative and positive charges; and when pH < 3.3, tetracycline molecules carry a positive charge [41]. Therefore, this experiment investigated the effects of pH values of 5, 7, 8, and 11 on the removal efficiency of TC by nCo@nZVI nanomaterials. The other experimental conditions are a temperature of 20 ℃, an initial TC concentration of 30 mg/L, and a nCo@nZVI nanomaterial dosage of 1 g/L.

The experimental results indicate that at low initial concentrations, nCo@nZVI nanomaterials exhibit high adsorption rates across a wide pH range. When the initial pH of the solution is 7, the TC removal rate reaches 81.01% after 120 minutes of adsorption. However, as the pH gradually increased to 11, the removal rate ultimately decreased to 46.33%, showing that the removal efficiency of TC gradually decreases, which is consistent with the typical characteristics of the Fenton reaction[42]. The lower the pH value, the less likely it is for a passivation layer to form on the Fe⁰ surface, leading to a faster corrosion rate and a large amount of iron ions dissolving out of the solution[43]. At pH = 3, iron ions may undergo coordination reactions with tetracycline, leading to tetracycline polymerization and precipitation, accompanied by the adsorption and reduction effects of nCo@nZVI nanomaterials, resulting in a fast reaction rate.

When the initial pH value increases to 8 and 11, tetracycline exists in the form of an anion, while nano iron carries a negative charge on its surface at pH > 8, which is not conducive to the adsorption of TC by nCo@nZVI nanomaterials[45]. As the pH value increases, iron ions will also be converted into $Fe(OH)_3$ or $Co(OH)_2$ precipitates, covering the surface of nCo@nZVI nanomaterials and hindering the further progress of reactions. Therefore, at higher pH values, the removal efficiency of TC is poor[44].

3.4 The Influence of Temperature

At a pH value of 7 and an initial TC concentration of 30 mg/L, the effect of temperature on the adsorption process of TC was studied using nCo@nZVI nanomaterials at a dosage of 1 g/L. The ambient temperatures during adsorption were varied (293.15 K, 313.15 K, 333.15 K). Figure 7 shows the characteristics of the adsorption process at different temperatures. It can be seen from the graph that as the temperature increases, the removal rate of TC by nCo@nZVI nanomaterials also increases. Although the removal rate of TC in the coupled system does not change significantly with the increase in reaction temperature, higher temperatures can accelerate the reaction process of TC. When the temperature increased from 293.15 K to 333.15 K, the removal rate of TC increased from 81.01–90.69% after about 120 min of adsorption.

In the low-temperature region (< 333.15 K), heating will intensify the diffusion process of oxygen, thereby accelerating the corrosion of nCo@nZVI nanomaterials, which increases the surface area and the number of active sites of the adsorbent. Additionally, an increase in temperature will increase the number of activated molecules, making it easier for TC to migrate from the solution to the surface of the adsorbent, accelerating the adsorption process and enhancing the accessibility of active sites on the surface of nCo@nZVI nanomaterials [46]. After 120 min of reaction, the removal rate of tetracycline by the coupled system was above 80%, indicating that the coupled system can adapt to a wide temperature range, which is of great significance for practical engineering applications.

3.5 Reaction Kinetics

3.5.1 Quasi First and Second-Order Kinetic Models

To gain insights into the removal process and mechanism of TC (tetracycline) adsorption by nCo@nZVI, linear fitting of adsorption kinetic data was conducted using both pseudo-first-order and pseudo-second-order kinetic models. The experiments were based on varying initial concentrations of TC (20 mg/L, 30 mg/L, 40 mg/L, and 50 mg/L), and these kinetic models were applied to fit the experimental data, simulating the TC removal process at multiple time points (5, 10, 20, 30, 60, 120, and 240 minutes).

Figure 8 visually presents the linear fitting results of the pseudo-first-order and pseudo-second-order kinetic models for the TC removal process. Upon comparison, it was found that the correlation coefficient of the pseudo-second-order kinetic model (R_2^2 = 0.99787) was higher than that of the pseudo-first-order kinetic model (R_1^2 = 0.98095), indicating that the adsorption process conforms better to the pseudo-second-order kinetic model, suggesting that the adsorption of TC by nCo@nZVI is primarily chemical in nature. Generally, the pseudo-first-order equation is primarily used to describe the initial stage of adsorption, whereas the pseudo-second-order equation encompasses more complex adsorption processes such as liquid film diffusion, surface adsorption, intraparticle diffusion, and electron sharing or transfer. Therefore, the pseudo-second-order kinetic model provides a more reasonable explanation for the adsorption process of TC by nCo@nZVI, which is also the general kinetic law for the removal of TC by nanoscale zero-valent iron composites.

Furthermore, the experiments observed that as the initial concentration of TC increased, the removal rate accelerated, and the time required to reach equilibrium decreased. This suggests that rate-controlling steps may play a pivotal role in the adsorption process [33, 47]. In chemical adsorption, the adsorption capacity is directly proportional to the number of active sites on the adsorbent surface; thus, as the initial pollutant concentration increases, the kinetic characteristics of removal also change [48]. The kinetic parameters obtained through linear regression analysis are shown in Table 1, revealing that higher initial concentrations result in higher ultimate adsorption capacities (q_e).

Table 1
Kinetic parameters obtained by linear regression analysis

Heavy metal ion	Initial concentration/(mg/L)	q_e/(mg·g^{-1})	R^2
TC	20	20	0.98338
	30	24.30253	0.98273
	40	25.02158	0.99247
	50	25.33313	0.99787

3.5.2 Internal diffusion model

To elucidate the roles of boundary layer diffusion (external mass transfer) and intraparticle diffusion (internal surface diffusion) in the adsorption mechanism, an intraparticle diffusion model analysis was conducted on the kinetic data. If intraparticle diffusion is the sole rate-controlling step, the fitted line would pass through the origin. Otherwise, boundary layer diffusion partially controls the adsorption process[49] [50].

Figure 9 presents the linear fitting results of the intraparticle diffusion model for the TC removal process at 20°C. The adsorption process of TC is nonlinear throughout the entire time range, indicating that multiple processes influence the adsorption. No distinct diffusion stage was observed in the three experiments, suggesting that under the experimental conditions, the adsorption of TC on nCo@nZVI nanomaterials is likely dominated by surface adsorption. The first stage (I) is attributed to surface diffusion resulting from surface complexation and instantaneous electron transfer. In the second stage (II), as the concentration of metal ions decreases, the internal transfer of TC from the boundary to the cores of nCo@nZVI nanomaterials becomes relatively slow. The final stage (III) is a slow and stable equilibrium process, possibly due to increased cation repulsion[51] [52]. However, the overall TC removal curve is not linear, indicating that intraparticle diffusion is only a secondary rate-limiting step, with other mechanisms such as surface mass transfer or degradation likely also playing a role[53].

3.6 Reaction Thermodynamics

Thermodynamic parameters play a pivotal role in assessing the feasibility of adsorption processes. In this study, Van't Hoff plots of lnk_C versus 1/T were constructed to thoroughly investigate the energy

conversion and spontaneous reaction characteristics involved in the binding process between nCo@nZVI nanomaterials and TC, through the analysis of entropy change (ΔS^0), enthalpy change (ΔH^0), and standard free energy change (ΔG^0). As clearly illustrated in Fig. 10, all Van't Hoff plots exhibited good linear correlations. Based on this linear relationship, precise values of $\Delta H^0$and ΔS^0 were accurately calculated using the results of linear fitting.

The fitted ΔH0 value was positive, which is attributed to the endothermic nature of the chemical adsorption process occurring between nCo@nZVI nanomaterials and TC [54], consistent with experimentally observed phenomena. In other words, as the adsorption ambient temperature increases, the removal efficiency of TC is enhanced.

From the relevant data tables, it can be observed that the calculated ΔG0 values were all negative and further decreased with increasing temperature. This trend not only confirms the promotion of adsorption reactions by elevated temperatures but also validates the practical feasibility of the removal process, clearly indicating that the adsorption process is spontaneous.

The positive ΔS^0 value to some extent reveals structural changes between the adsorbate (TC) and adsorbent (nCo@nZVI nanomaterials), indicating that the adsorption process leads to an increase in the disorder and randomness of the system, i.e., the adsorption proceeds in the direction of entropy increase. This change may suggest the occurrence of some chemical interaction between TC and nCo@nZVI nanomaterials, further highlighting the strong affinity of nCo@nZVI nanomaterials for TC [50]. Additionally, the positive ΔS^0 value typically implies the possible release of solvent molecules (such as H_2O) during the adsorption of tetracycline molecules onto the surface of nCo@nZVI nanomaterials. These released solvent molecules enter the solution phase, increasing the entropy of the entire system, which also partially explains the positive ΔH0 value, indicating that this adsorption process is endothermic and requires the absorption of heat to maintain the reaction [55]. Notably, the relationship $|\Delta H^0| < |T \bullet \Delta S^0|$ shown in the data further indicates that entropy effects dominate over enthalpy effects in this adsorption process. Therefore, it can be concluded that this adsorption process is primarily controlled by entropy.

Table 2
Thermodynamic fitting results of TC adsorption by nCo@nZVI

Pollutant	*T*/K	ΔS^0/(J/mol/K)	ΔH^0/(KJ/mol)	ΔG^0/(KJ/mol)
TC	293.15	88.3057	22.975	-2.804
	313.15			-4.923
	333.15			-6.305

3.7 Adsorption Isotherm

The adsorption process is usually described using Langmuir and Freundlich isotherms to characterize the interaction between the adsorbent and the adsorbate. In this study, data were obtained from the equilibrium results of the kinetic study, and a chart was plotted at 20°C to show the adsorption capacity of TC and the corresponding adsorption equilibrium concentration, resulting in an adsorption isotherm. Subsequently, these data were applied to Langmuir and Freundlich models, as shown in Fig. 11.

By using the Langmuir model, we can determine the maximum adsorption capacity q_{max} of nCo@nZVI nanomaterials for different concentrations of TC, which is 25.33313 mg/g. The experimental data and the fitting results of the Langmuir model have a higher $\mathbf{R}^2_{\mathrm{Langmuir}} = 0.99268$ compared to the Freundlich model $\mathbf{R}^2_{\mathrm{Freundlich}} = 0.94444$, indicating that the interaction between nCo@nZVI nanomaterials and TC is primarily chemical adsorption[56]. The adsorption process aligns more closely with the Langmuir model's assumption of single-layer and uniform adsorption. In other words, the adsorbent surface has equal binding energy, and there is no interaction between the adsorbates, resulting in TC being fixed on the surface of nCo@nZVI nanomaterials in a monolayer form.

3.8 nCo@nZVI Removing tetracycline mechanism

Based on previous experimental results, this article proposes a plausible mechanism for the removal of tetracycline (TC), as illustrated in Fig. 12. The mechanism involves the following steps: First, TC is adsorbed onto the surface of nCo@nZVI through electrostatic interactions. Second, due to the presence of active groups such as -OH and -NH_2 in TC molecules, and the unsaturated metal sites on nCo@nZVI, TC interacts with the adsorbent via ion exchange. Additionally, nCo@nZVI can activate H□O□ to trigger Fenton-like reactions (see equations (1) and (2)), further degrading TC.

Upon introduction of nCo@nZVI into the TC solution, TC adheres to the surface of the material through electrostatic and functional group interactions. Being a nanoscale material with a large specific surface area, nCo@nZVI effectively adsorbs TC, and the nZVI in its core-shell structure facilitates further TC removal through its reducing effect. Hydroxyl radicals (·OH), the primary reactive oxygen species (ROS), are generated through two main pathways: Fe²□ in the system activates H_2O_2 to produce ·OH, and nZVI on the material surface directly reacts with H_2O_2 to generate ·OH (see Eq. (3)) [57]. Consequently, Fe^0, Fe^{2+}, and Fe^{3+} in the system are efficiently cycled. Replacing Fe²□ with nCo@nZVI in traditional Fenton reactions promotes Fe²□ cycling with reduced toxicity. In the nCo@nZVI-catalyzed Fenton-like reaction, H_2O_2 activation promotes the interconversion of iron in different valence states, reduces the formation of iron hydroxides, and enhances ·OH generation. ·OH oxidizes TC, ultimately degrading it into CO_2 and H_2O. Figure 12 depicts the degradation mechanism of TC in the Fenton-like reaction system catalyzed by nCo@nZVI nanomaterials [58].

$$\mathbf{Fe^0 + O_2 + 2H^+ \rightarrow\ Fe^{2+} + H_2O_2}$$

1

$$\mathbf{Fe}^{0} + \mathbf{H_2O_2} + 2\mathbf{H}^{+} \rightarrow \mathbf{Fe}^{2+} + 2\mathbf{H_2O}$$

2

$$\mathbf{Fe}^{2+} + \mathbf{H_2O_2} \rightarrow \mathbf{Fe}^{3+} + \mathbf{OH}^{-} + \bullet\,\mathbf{OH}$$

3

The TC molecules are primarily oxidized and decomposed through functional group loss and ring-opening processes, including demethylation, hydroxylation, dehydroxylation, and amide bond cleavage. These degradation processes were analyzed using liquid chromatography, with the possible pathways illustrated in Fig. 13. Initially, TC may undergo dehydroxylation to form product (a) (m/z = 427), followed by ring opening to yield product (c) (m/z = 298), and further degradation through ring-opening oxidation. Another potential pathway involves the cleavage of TC into 2 N-methyl groups, 2 ammonium groups, and 2 hydroxyl groups, resulting in product (b) (m/z = 330). Due to the weak bond energy of the N-methyl group, it is prone to cleavage, leading to product (d) (m/z = 270) through further breakdown of hydroxyl and formyl groups from product (b) [61]. As the reaction progresses, the types and quantities of intermediate products increase, with larger molecules being continuously oxidized and decomposed into smaller molecules, ultimately resulting in CO₂ and H₂O. Additional degradation pathways may produce various other degradation products.

3.9 Magnetic Separation of nCo@nZVI

Figures 13(b) and (c) illustrate the dispersion effect observed during the shaking of the nCo@nZVI nanomaterials mixed with tetracycline (TC), as well as the magnetic separation effect achieved by the application of an external magnetic field on the nCo@nZVI nanomaterials. The research results indicate that nCo@nZVI nanomaterials have good dispersion in TC solution, likely due to their magnetic properties. As shown in the figures, after treatment, nCo@nZVI nanomaterials exhibit good magnetism, making them easy to recycle and process. Furthermore, the utilization of an external magnetic field significantly accelerates the separation of nCo@nZVI nanomaterials from pollutants, thereby reinforcing the practical viability of efficiently retrieving nCo@nZVI nanomaterials through magnetic separation technology[62].

To achieve the reuse of nCo@nZVI nanomaterials, the following steps were taken to regenerate the materials after the reaction: first, use the method of wrapping a magnet with cling film to remove the used nCo@nZVI nanomaterials, then place them in a beaker containing deionized water and stir and rinse four times. The same method is used to remove the cleaned material, which is then placed in 0.1 mol/L hydrochloric acid to regenerate nCo@nZVI nanomaterials[63]. According to the results in Fig. 13(a), at a TC concentration of 20 mg/L, the removal rate of TC gradually decreases with the increase in regeneration cycles, with the decrease becoming more pronounced. After the fifth regeneration, the removal rate decreased to 65.87%. In summary, nCo@nZVI nanomaterials, as effective pollutant removal

agents, have the potential to achieve efficient recovery through magnetic separation technology and are of great significance for practical applications.

4 Conclusion

This study explores an inexpensive and simple method for preparing magnetic sheet-like materials nCo@nZVI Nanomaterial materials have been used to solve the problem of antibiotic contamination in wastewater. This method avoids problems such as the use of expensive reducing agents. By employing a diverse array of methodologies, the physicochemical properties and intricate fine structure of the material were meticulously characterized, thereby offering a novel approach for the utilization of cobalt in wastewater. In the experiment, the influence of various factors on the removal efficiency of tetracycline was examined, and multiple classical models were used to analyze the removal process. Through research, the following conclusions have been drawn:

(1) Preparation by rheological phase reaction nCo@nZVI Nanomaterial composite materials, in which nZVI particles form a single sheet-like structure, and $CoFe_2O_4$ exhibits a radioactive shape. Upon further magnification, it was observed that the structure was clearly rod-shaped, with a length ranging from 100 to 2000 nm and a thickness less than 100 nm.

(2) nCo@nZVI nanomaterials are employed for the removal of TC. Experimental results indicate that, at a pH of 7 and a temperature of 20°C, with the addition of 1 g/L of these nanomaterials, it takes approximately 120 minutes to reduce the TC content in wastewater with an initial concentration of 20 mg/L to trace levels. While increasing the initial TC concentration results in a decrease in removal efficiency, it positively impacts the adsorption capacity of the nanomaterials.

(3) During the TC removal process utilizing nCo@nZVI nanomaterials, the kinetics adhere to a pseudo-second-order model, whereas the adsorption isotherm conforms more closely to the Langmuir model, suggesting that the process involves chemical adsorption. The adsorption capacity of TC, calculated using the Langmuir model, reaches 25.33313 mg/g. Thermodynamic analysis indicates that this removal process is spontaneous. The enrichment of TC by nCo@nZVI nanomaterials is primarily achieved through an adsorption-degradation mechanism.

(4) Under the condition of a TC concentration of 20 mg/L, the nCo@nZVI nanomaterial maintained a removal efficiency of 65.87% even after the fifth cycle of regeneration. This indicates that nCo@nZVI not only demonstrates excellent performance in pollutant removal but also exhibits remarkable stability during repeated use. More importantly, the material's potential for efficient recovery through magnetic separation is significant for the recycling of cobalt-containing wastewater, contributing to the development of a comprehensive circular green recovery system. This feature is expected to reduce operational costs, enhance resource utilization, and provide a sustainable solution for environmental remediation.

Declarations

Author Contribution

A: Conceptualization, Methodology, Software, Formal Analysis, Writing - Original Draft Visualization;B: Resources, Investigation, Supervision;C: Data Curation, Funding Acquisition, Writing - Original Draft;D: Investigation; Conceptualization, Funding Acquisition, Resources, Supervision ;E: Resources, Investigation;F: Software, Validation,Writing - Review & Editing;G: Visualization, Writing - Review & Editing;H: Investigation;I: Resources;All authors reviewed the manuscript.

Acknowledgements

We are grateful to the sponsors of this work. Anhui University of Technology, School of Metallurgical Engineering and School of Materials Science and Engineering, Jiuquan Vocationl and Technical College, Key Laboratory of Metallurgical Emission Reduction & Resources Recycling (Ministry of Education), Anhui Provincial Central Leading Local Science and Technology Development Special Project (No. 202107d06050012); Anhui University Graduate Scientific Research Project (No. YJS202110333); Gansu Province University Teacher Innovation Fund Project, (No. 2024B-342), Natural Science Foundation of Gansu Province, (No. 24JRRF006)

References

1. KUMAR M, SRIDHARAN S, SAWARKAR A D, et al. Current research trends on emerging contaminants pharmaceutical and personal care products (PPCPs): A comprehensive review [J]. Science of The Total Environment, 2023, 859: 160031.
2. NANDI A, PECETTA S, BLOOM D E. Global antibiotic use during the COVID-19 pandemic: analysis of pharmaceutical sales data from 71 countries, 2020–2022 [J]. eClinicalMedicine, 2023, 57: 101848.
3. HENA S, GUTIERREZ L, CROUé J-P. Removal of pharmaceutical and personal care products (PPCPs) from wastewater using microalgae: A review [J]. Journal of Hazardous Materials, 2021, 403: 124041.
4. SCARIA J, ANUPAMA K V, NIDHEESH P V. Tetracyclines in the environment: An overview on the occurrence, fate, toxicity, detection, removal methods, and sludge management [J]. Science of The Total Environment, 2021, 771: 145291.
5. ZHANG X, CAI T, ZHANG S, et al. Contamination distribution and non-biological removal pathways of typical tetracycline antibiotics in the environment: A review [J]. Journal of Hazardous Materials, 2024, 463: 132862.
6. YAN L, SONG X, MIAO J, et al. Removal of tetracycline from water by adsorption with biochar: A review [J]. Journal of Water Process Engineering, 2024, 60: 105215.

7. YANG L, YUAN C, CHEN X, et al. The effect of nitrification inhibitors on the aerobic biodegradation of tetracycline antibiotics in swine wastewater [J]. Chemosphere, 2023, 311: 136849.
8. ZHENG J, ZHANG P, LI X, et al. Insight into typical photo-assisted AOPs for the degradation of antibiotic micropollutants: Mechanisms and research gaps [J]. Chemosphere, 2023, 343: 140211.
9. YOU C-S, JUNG S-C. Photo-catalytic destruction of tetracycline antibiotics using terbium and manganese co-precipitated TiO2 photocatalyst [J]. Journal of Environmental Chemical Engineering, 2024, 12(1): 111666.
10. ZENG S, KAN E. Comparative insights into performance and mechanisms of Fenton and persulfate oxidation on iron-functionalized activated biochar for removal of aqueous tetracycline antibiotics [J]. Journal of Water Process Engineering, 2024, 65: 105824.
11. LIU F, ZHANG H, LIU N, et al. Enhanced removal of refractory organic pollutants in wafer surface treatment wastewater by combining Fenton oxidation and O_3/H_2O_2/FeOOH: Removal efficiency, intermediate composition, and toxicity prediction [J]. Journal of Water Process Engineering, 2024, 64: 105572.
12. ZAFAR A M, JAVED M A, HASSAN A A, et al. Groundwater remediation using zero-valent iron nanoparticles (nZVI) [J]. Groundwater for Sustainable Development, 2021, 15: 100694.
13. LIU M, CHEN G, XU L, et al. Environmental remediation approaches by nanoscale zero valent iron (nZVI) based on its reductivity: a review [J]. RSC Advances, 2024, 14(29): 21118–38.
14. KEN D S, SINHA A. Recent developments in surface modification of nano zero-valent iron (nZVI): Remediation, toxicity and environmental impacts [J]. Environmental Nanotechnology, Monitoring & Management, 2020, 14: 100344.
15. AKBARZADEH F Z, SARRAF M, GHOMI E R, et al. A state-of-the-art review on recent advances in the fabrication and characteristics of magnesium-based alloys in biomedical applications [J]. Journal of Magnesium and Alloys, 2024.
16. Z Y CAO. Synthesis of Fe,Co-based Subnano cluster catalysts and their oxygen reduction reaction performance [D]. Heilongjiang:Northeast Petroleum University 2023.(in Chinese)
17. Y Y CUI. Iron cobalt bimetallic co modified carbon nanotube film effectively removes tetracycline [D]. Shanghai: Shanghai Normal University 2024. (in Chinese)
18. Y CUI. Degradation of the Micro-Medicine in Water by Carbon-Based Loaded Iron-Cobalt Nanosphere Activated Persulfate [J]. TECHNOLOGY OF WATER TREATMENT. 2023, 49(11): 73–9. (in Chinese)
19. YANG Ruiming,TANG Yani,LI Jingwen,et al.Study the Adsorption of Nitrate in Water by Cobalt□Iron Layered Bimetal□Loaded Biochar[J].Journal of Petrochemical Universities,2024,37(2):16–23. (in Chinese)
20. CHEN M, LIU D, ZI B, et al. Remarkable synergistic effect in cobalt-iron nitride/alloy nanosheets for robust electrochemical water splitting [J]. Journal of Energy Chemistry, 2022, 65: 405–14.
21. XIE W, SHI Y, WANG Y, et al. Electrospun iron/cobalt alloy nanoparticles on carbon nanofibers towards exhaustive electrocatalytic degradation of tetracycline in wastewater [J]. Chemical Engineering Journal, 2021, 405: 126585.

22. KILANSKI L, LEWINSKA S, SLAWSKA-WANIEWSKA A, et al. Attempts to obtain BaTiO3/Fe2O3 core-shell type structures: The role of iron oxide nanoparticle formation and agglomeration [J]. Inorganic Chemistry Communications, 2022, 145: 109960.
23. W B WANG. The preparation of iron-cobalt bimetal composite carbon felt electrodes and its electro-Fenton treatment for dye wastewater [D], Dalian: Dalian Maritime University 2023. (in Chinese)
24. KAMRANIFAR M, ALLAHRESANI A, NAGHIZADEH A. Synthesis and characterizations of a novel $CoFe_2O_4$@CuS magnetic nanocomposite and investigation of its efficiency for photocatalytic degradation of penicillin G antibiotic in simulated wastewater [J]. Journal of Hazardous Materials, 2019, 366: 545–55.
25. LEE M, YOON G, KIM M K, et al. Synthesis of amorphous cobalt hydroxide nanosheets and electrochemical performance according to phase transition into crystalline cobalt oxides [J]. Journal of Alloys and Compounds, 2024, 976: 173282.
26. D Yu, P Y CAI, H B CHENG, et al. Preparation of nanomaterials ZIF-8@TOCN andadsorption of Rhodamine B [J] TEXTILE AUXILIARIES. 2024, 41(05): 18–22. (in Chinese)
27. CARRERA ESPINOZA M J, LIN K-S, WENG M-T, et al. In vitro studies of Pluronic F127 coated magnetic silica nanocarriers for drug delivery system targeting liver cancer [J]. European Polymer Journal, 2021, 153: 110504.
28. HU J, CHEN G, LO I M C. Removal and recovery of Cr(VI) from wastewater by maghemite nanoparticles [J]. Water Research, 2005, 39(18): 4528–36.
29. WANG X, ZHENG Y, NING P, et al. Synergetic effect of green synthesized NZVI@Chitin-modified ZSM-5 for efficient oxidative degradation of tetracycline [J]. Environmental Research, 2024, 258: 119360.
30. S HAN. degradation of tetracycle by activated of peroxymonosulfate using pomelo peel biochar loaded with iron cobalt bimetallic catalyst [D], Heilongjiang: Northeast Forestry University 2022. (in Chinese)
31. D AI, T Q WEI, YA MENG, et al. Study on Adsorptionzero Effect of Zero□Valent Iron/Cationic Surfactant/Biochar on Cr(VI) [J]. JOURNAL OF PETROCHEMICAL UNIVERSITIES, 2022, 35(03): 54–62. (in Chinese)
32. S Cao. Remediation effect and mechanism of cadmium in paddy soil by biochar supported sulfurized nano zero valent iron [D], 2023. (in Chinese)
33. ZHANG X, HE Y, GAO G, et al. Novel core-shell structural nZVI@Fe2P for sulfadiazine (SDZ) degradation: Accelerated Fe(III)/Fe(II) dynamic cycling, boosted Fenton performance and stability [J]. Separation and Purification Technology, 2024, 347: 127705.
34. IBRAR S, ABDULLAH, ASHFAQ H, et al. A step forward towards optimized iron–nickel bimetal oxide core–shell nanoparticles and their magnetic properties [J]. Materialia, 2024, 36: 102135.
35. X S GAO, G S LIU, F QIN, et al. Porous Cobalt-Iron Binary Metal Oxides Nanorods as Efficient Oxygen Evolving Catalysts for Water Splitting [J].Chinese Journal of inorganic chemistry,2017, 33(04): 623–9. (in Chinese)

36. WEN M, SUN Y, LI X, et al. Ru-capped/FeCo nanoflowers with high catalytic efficiency towards hydrolytic dehydrogenation [J]. Journal of Power Sources, 2013, 243: 299–305.
37. QIU S, WANG Y, WAN J, et al. Enhanced electro-Fenton catalytic performance with in-situ grown Ce/Fe@NPC-GF as self-standing cathode: Fabrication, influence factors and mechanism [J]. Chemosphere, 2021, 273: 130269.
38. YANG W, ZHU Y, YOU F, et al. Insights into the surface-defect dependence of molecular oxygen activation over birnessite-type MnO_2 [J]. Applied Catalysis B: Environmental, 2018, 233: 184–93.
39. GOPAL G, SANKAR H, NATARAJAN C, et al. Tetracycline removal using green synthesized bimetallic nZVI-Cu and bentonite supported green nZVI-Cu nanocomposite: A comparative study [J]. Journal of Environmental Management, 2020, 254: 109812.
40. C H JING. Research Process and Expectation on the Treatment Technology of Tetracycline Antibiotics[J]. Shandong Chemical Industry. 2022, 51(18): 102–6. (in Chinese)
41. BAI S, ZHU S, JIN C, et al. Sorption mechanisms of antibiotic sulfamethazine (SMT) on magnetite-coated biochar: pH-dependence and redox transformation [J]. Chemosphere, 2021, 268: 128805.
42. TIAN G, NIE K, HAN G, et al. Iron ore tailings as efficient Fenton-like catalysts for degradation of tetracycline [J]. Materials Today Communications, 2023, 37: 107598.
43. CHI C, HUO B, LIANG Z, et al. Study on tetracycline degradation in wastewater based on zero-valent nano iron assisted micro-nano bubbles [J]. Alexandria Engineering Journal, 2024, 86: 577–83.
44. ZHOU L, ZHANG G, ZENG Y, et al. Endogenous iron-enriched biochar derived from steel mill wastewater sludge for tetracycline removal: Heavy metals stabilization, adsorption performance and mechanism [J]. Chemosphere, 2024, 359: 142263.
45. SUN Y-P, LI X-Q, ZHANG W-X, et al. A method for the preparation of stable dispersion of zero-valent iron nanoparticles [J]. Colloids and Surfaces A: Physicochemical and Engineering Aspects, 2007, 308(1): 60–6.
46. ARSHADI M, SOLEYMANZADEH M, SALVACION J W L, et al. Nanoscale Zero-Valent Iron (NZVI) supported on sineguelas waste for Pb(II) removal from aqueous solution: Kinetics, thermodynamic and mechanism [J]. Journal of Colloid and Interface Science, 2014, 426: 241–51.
47. LI W, ZHOU Z, CHEN Z, et al. Adsorption and degradation of tetracycline hydrochloride in aqueous solutions using activated carbon with Fe/Ag nanoparticles [J]. Materials Today Communications, 2024, 39: 108504.
48. ARSHADI M, ABDOLMALEKI M K, MOUSAVINIA F, et al. Nano modification of NZVI with an aquatic plant Azolla filiculoides to remove Pb(II) and Hg(II) from water: Aging time and mechanism study [J]. Journal of Colloid and Interface Science, 2017, 486: 296–308.
49. ISLAM M A, NAZAL M K, ANGOVE M J, et al. Emerging iron-based mesoporous materials for adsorptive removal of pollutants: Mechanism, optimization, challenges, and future perspective [J]. Chemosphere, 2024, 349: 140846.
50. YANG L, JIN X, LIN Q, et al. Enhanced adsorption and reduction of Pb(II) and Zn(II) from mining wastewater by carbon@nano-zero-valent iron (C@nZVI) derived from biosynthesis [J]. Separation

and Purification Technology, 2023, 311: 123249.

51. QU J, LIU Y, CHENG L, et al. Green synthesis of hydrophilic activated carbon supported sulfide nZVI for enhanced Pb(II) scavenging from water: Characterization, kinetics, isotherms and mechanisms [J]. Journal of Hazardous Materials, 2021, 403: 123607.
52. YAN J, LI K. A magnetically recyclable polyampholyte hydrogel adsorbent functionalized with β-cyclodextrin and graphene oxide for cationic/anionic dyes and heavy metal ion wastewater remediation [J]. Separation and Purification Technology, 2021, 277: 119469.
53. NGUYEN T C, LOGANATHAN P, NGUYEN T V, et al. Simultaneous adsorption of Cd, Cr, Cu, Pb, and Zn by an iron-coated Australian zeolite in batch and fixed-bed column studies [J]. Chemical Engineering Journal, 2015, 270: 393–404.
54. LIN Z, LIU F, ZHENG C, et al. Highly efficient removal of Cd(II) in aqueous solution by attapulgite-loaded amorphous zero-valent Iron [J]. Colloids and Surfaces A: Physicochemical and Engineering Aspects, 2023, 659: 130776.
55. CHEN M, XU H, ZHANG Y, et al. Effective removal of heavy metal ions by attapulgite supported sulfidized nanoscale zerovalent iron from aqueous solution [J]. Colloids and Surfaces A: Physicochemical and Engineering Aspects, 2022, 640: 128192.
56. ZHOU C, SUI M, GUO Y, et al. Enhancing Fenton-like reaction through a multifunctional molybdenum disulfide film coating on nano zero valent iron surface (MoS2@nZVI): Collaboration of radical and non-radical pathways [J]. Science of The Total Environment, 2024, 920: 170818.
57. X Y ZHANG, C Q HE, J Y JIANG, et al. Study Progress of Class-Fenton Treatment Technology [J]. ENVIRONMENTAL SCIENCE AND MANAGEMENT, 2015, 40(06): 58–61. (in Chinese)
58. X Z Xie. Treatment of sulfonamide antibiotics in water by Fenton-like process using ferriferrous oxide supported nano zero-valent iron [D], 2022. (in Chinese)
59. LIAQAT M, KHALID N R, IQBAL T, et al. Synthesis of heterojunction BiVO4/MnO_2 graphene ternary nanocomposites with enhanced photocatalytic activities through degradation of rhodamine B and tetracycline hydrochloride [J]. Chinese Journal of Physics, 2024, 91: 406–20.
60. TUNç M S, HANAY Ö. Removal of tetracycline antibiotic from aqueous solution using biosorbent [J]. Desalination and Water Treatment, 2022, 261: 308–21.
61. ZHANG M, SHANG Q, WAN Y, et al. Self-template synthesis of double-shell TiO2@ZIF-8 hollow nanospheres via sonocrystallization with enhanced photocatalytic activities in hydrogen generation [J]. Applied Catalysis B: Environmental, 2019, 241: 149–58.
62. NG W M, LIM J K. Complex interplay between colloidal stability, transport, chemical reactivity and magnetic separability of polyelectrolyte-functionalized nanoscale zero-valent iron particles (nZVI) toward their environmental engineering application [J]. Colloid and Interface Science Communications, 2022, 46: 100582.
63. VAN NGUYEN H, TUNG PHAM S, VU T N, et al. Effective treatment of 2,4,6-trinitrotoluene from aqueous media using a sono–photo-Fenton-like process with a zero-valent iron nanoparticle (nZVI)

catalyst Electronic supplementary information (ESI) available. [J]. RSC Advances, 2024, 14(33): 23720–9.

Figures

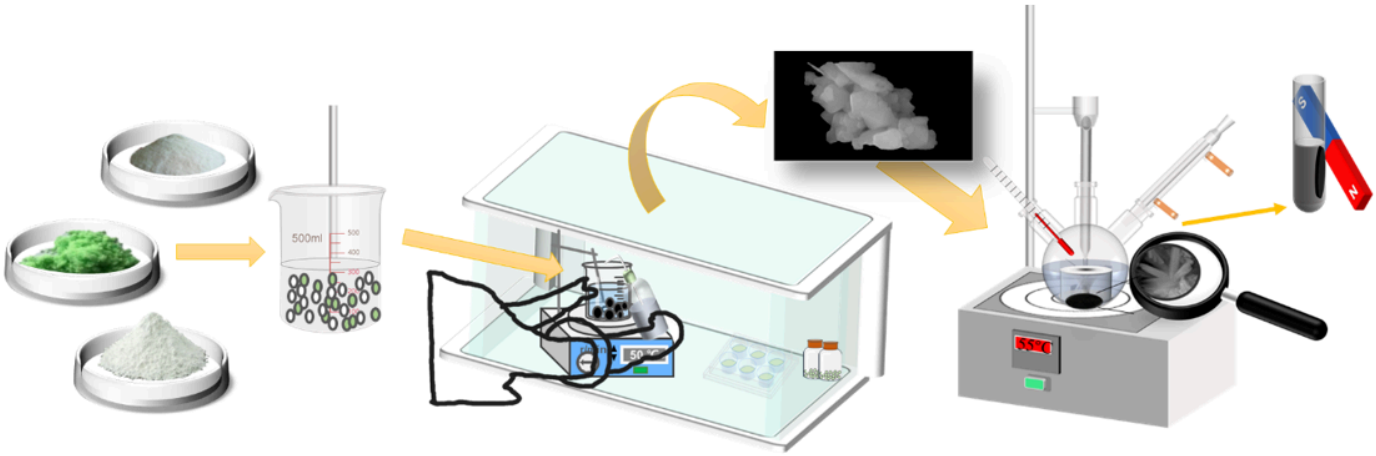


Figure 1

Preparation nCo@nZVI Schematic diagram of nanomaterials

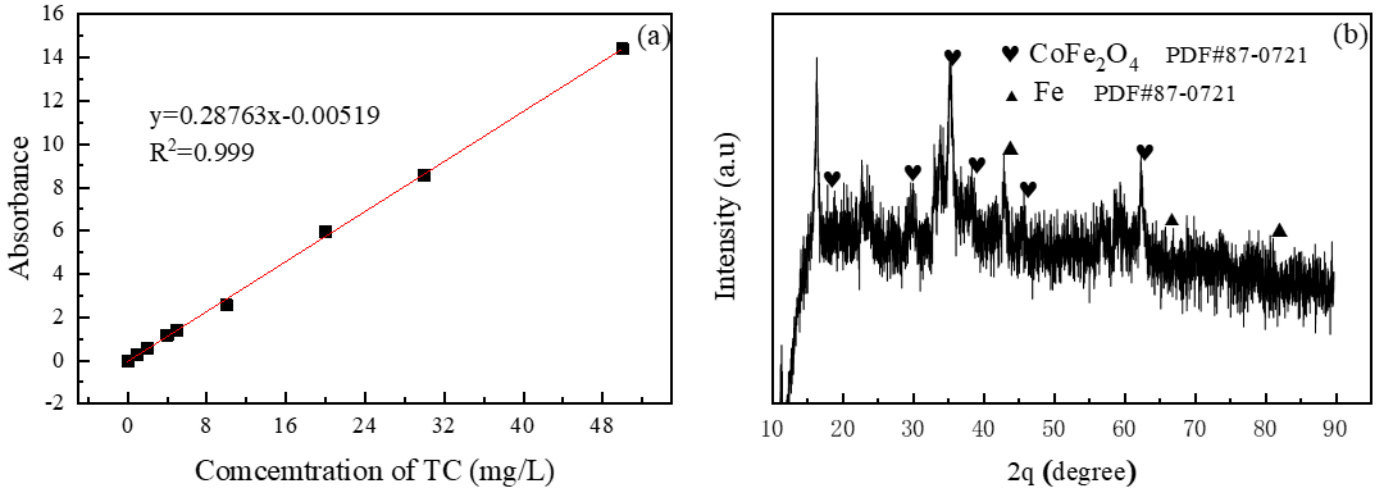


Figure 2

Standard curve of TC concentration (a), nCo@nZVI XRD pattern (b)

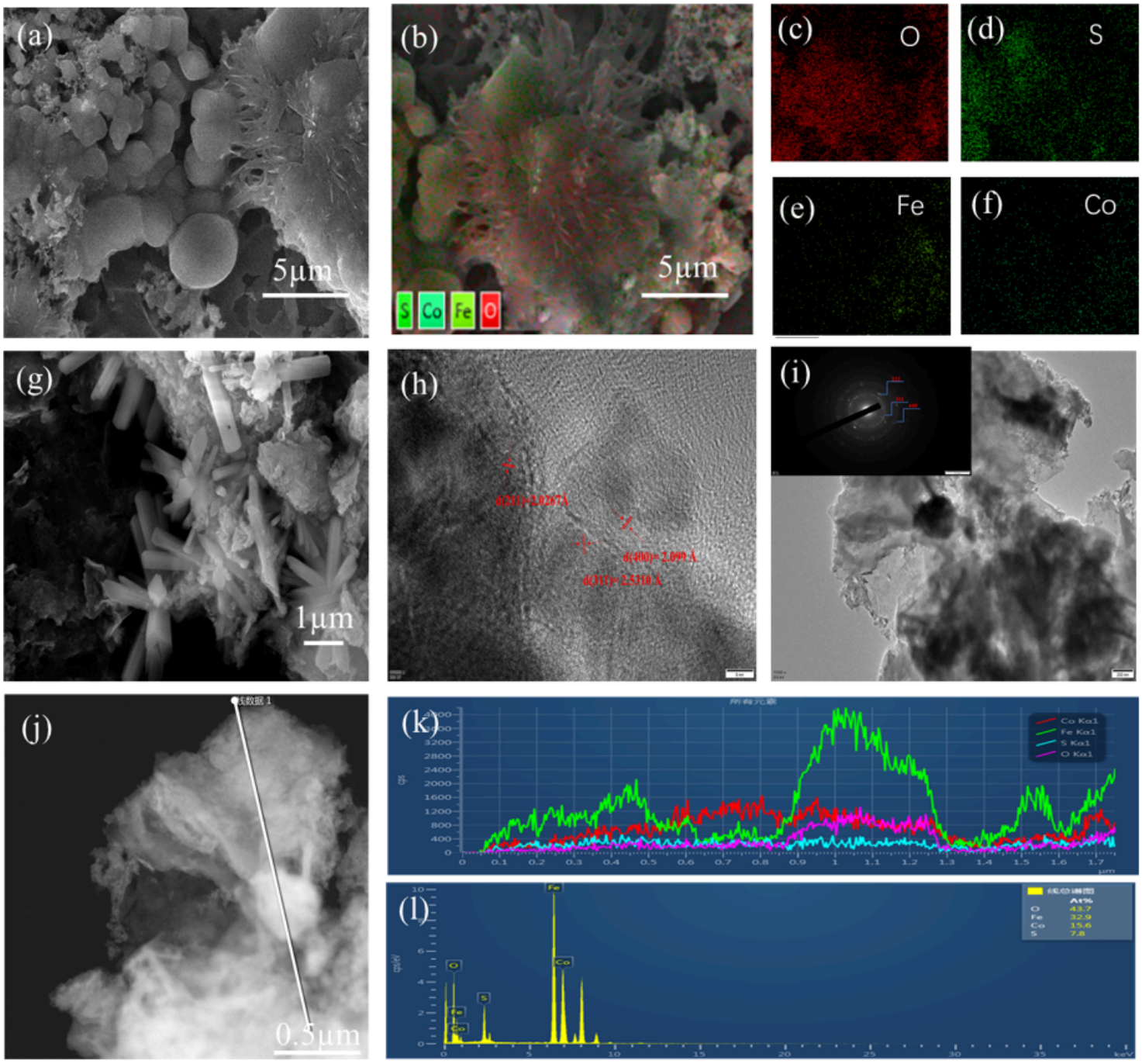


Figure 3

SEM images (a, b, g) of nCo@nZVI, EDS energy spectrum scanning (c-f), TEM images (h-j), and line scanning (k-l)

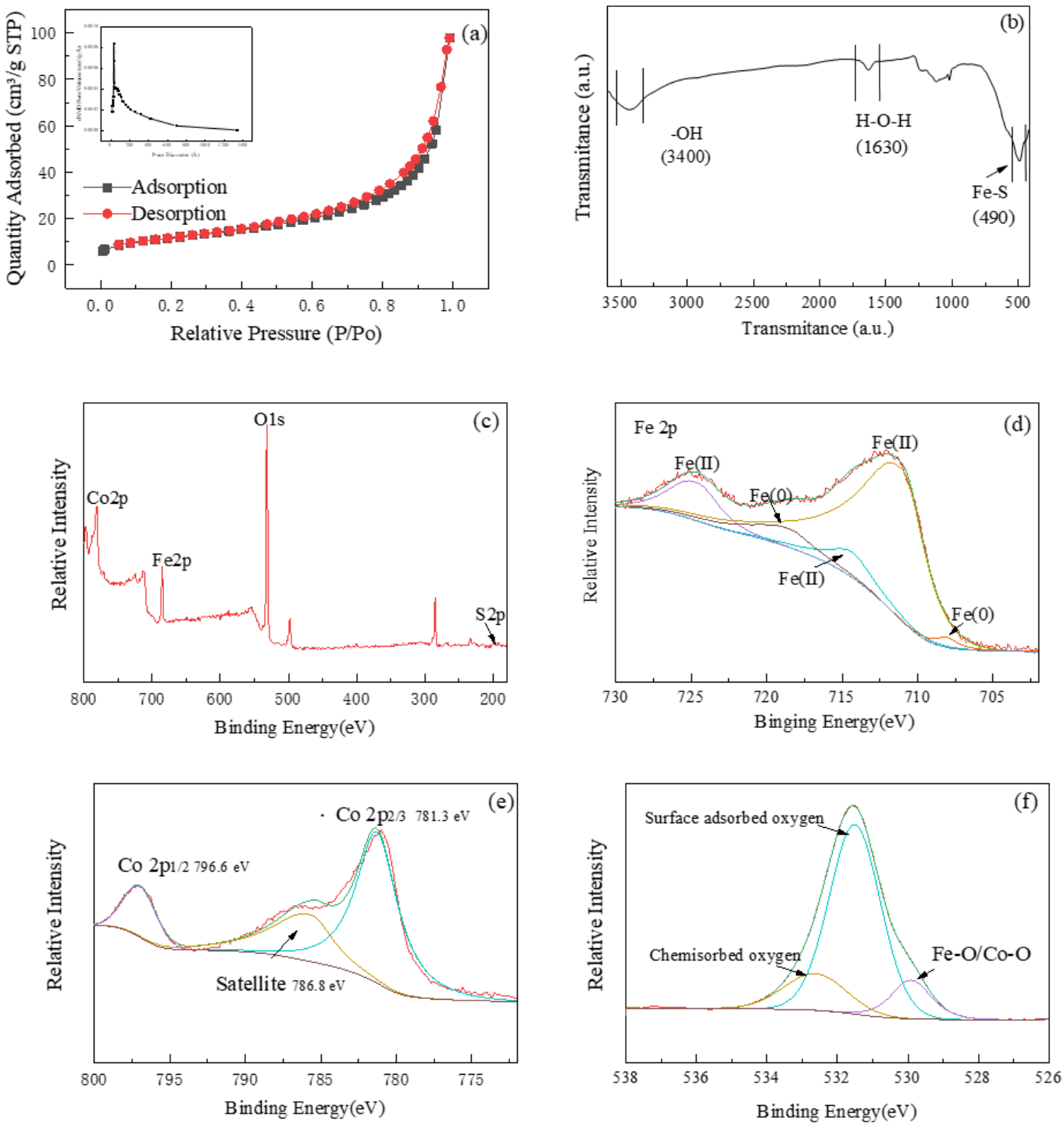


Figure 4

BET pattern of nCo@nZVI nanometer material (a). FTIR spectrum (b), XPS full spectrum (c), Fe 2p fine spectrum(d), Co 2p fine spectrum(e) and O1s fine spectrum (f)

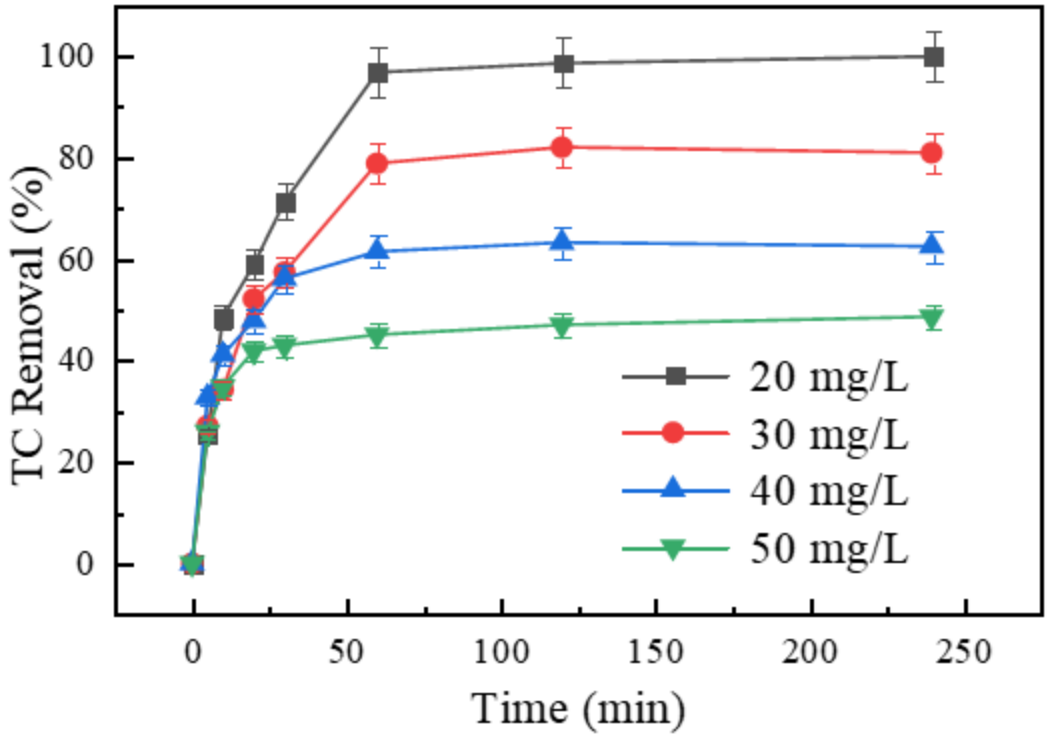


Figure 5

Variation in removal efficiency of different concentrations of TC during the removal process using nCo@nZVI

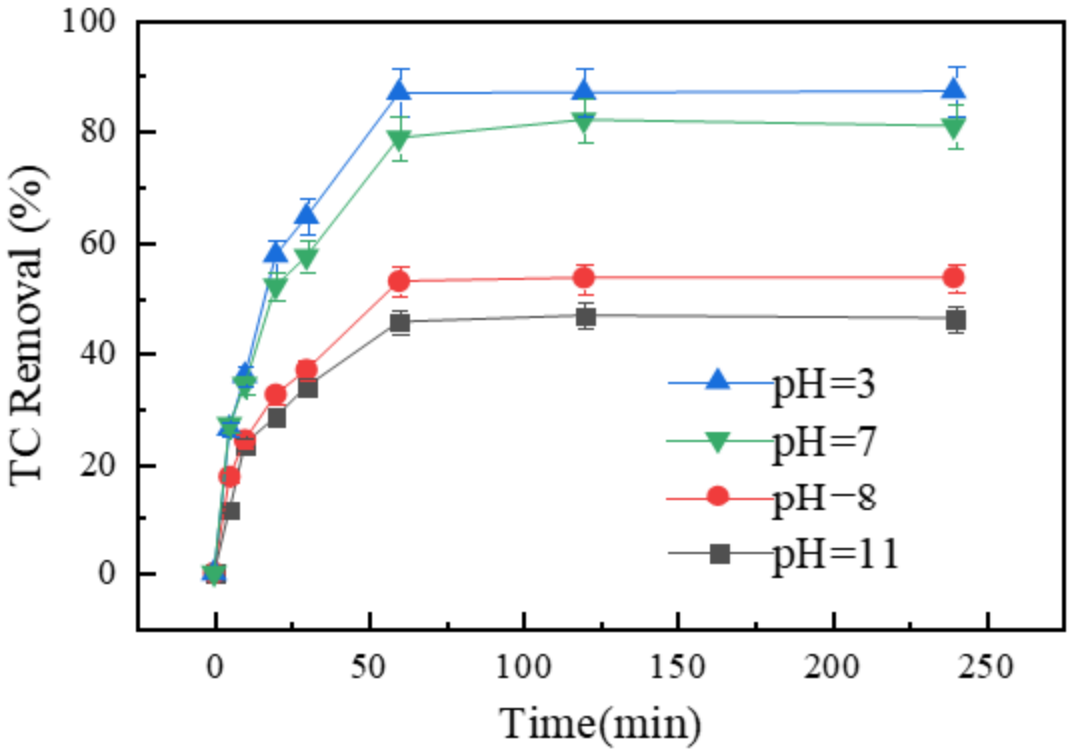


Figure 6

Influence of Initial pH on the Removal Efficiency of TC by nCo@nZVI

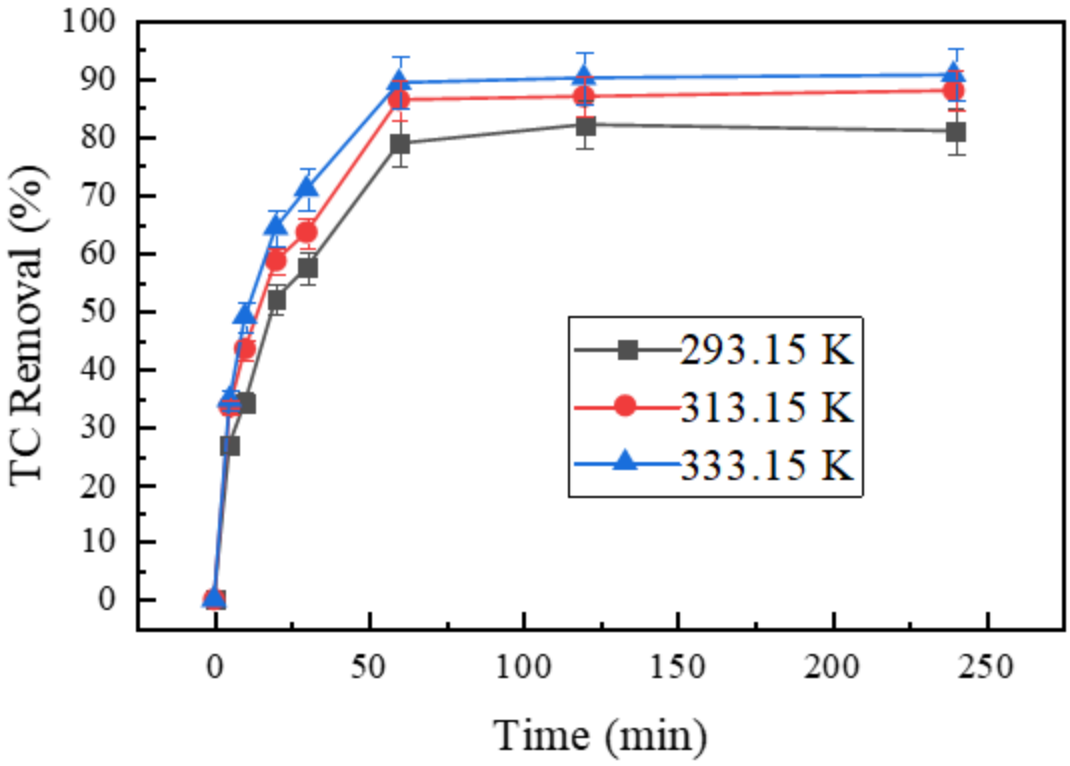


Figure 7

Impact of Temperature on the Removal Efficiency of TC by nCo@nZVI

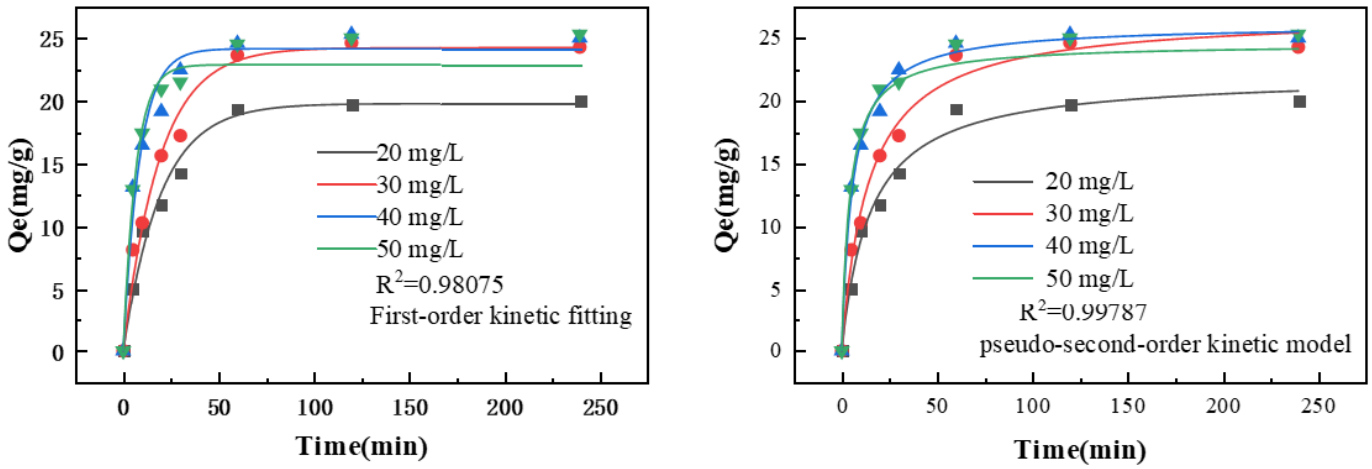


Figure 8

Quasi-secondary kinetic linear fitting results of TC removal process

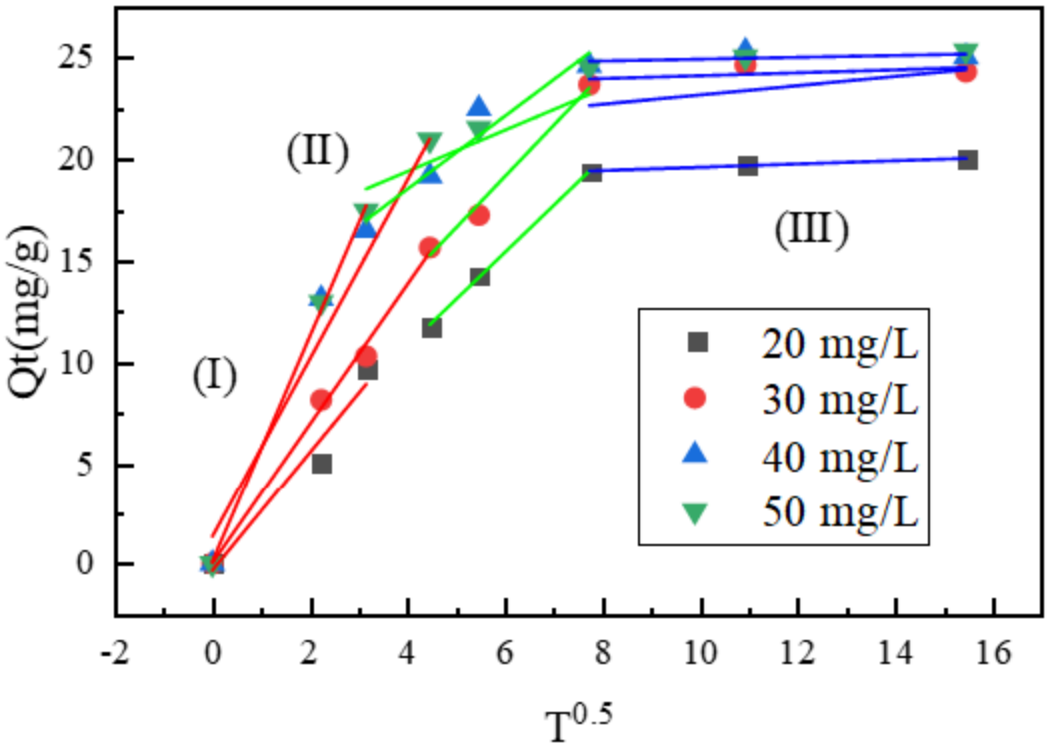


Figure 9

Linear Fitting Results of the Intra-particle Diffusion Model for the TC Removal Process

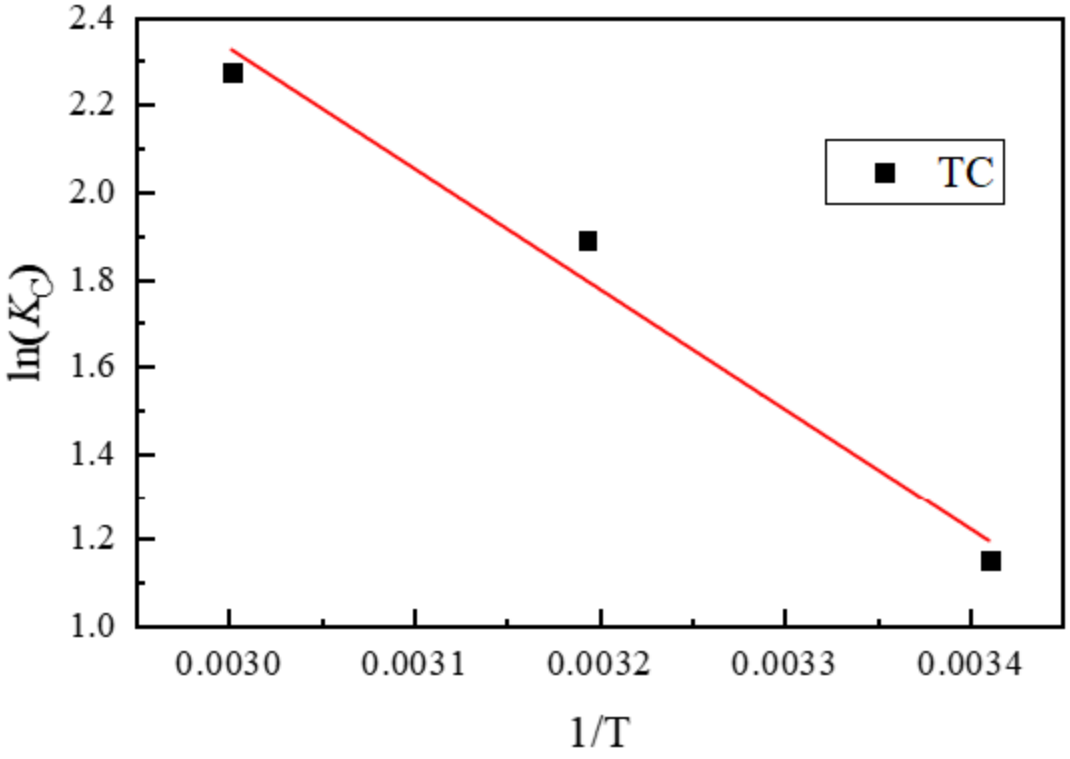


Figure 10

Van't Hoff plots of the adsorption results of nCo@nZVI on TC

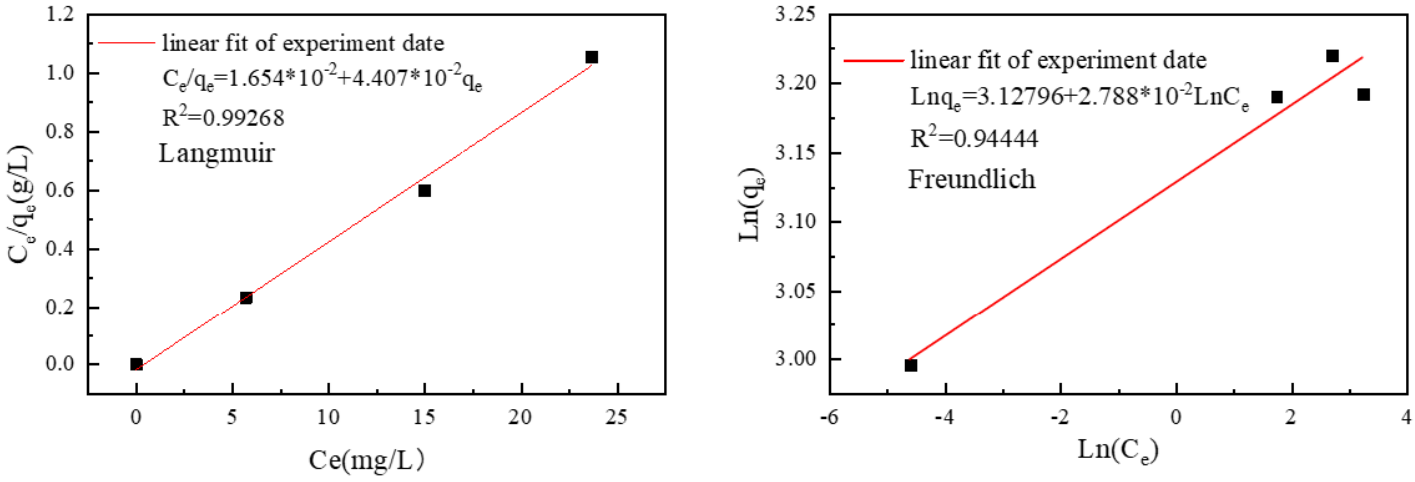


Figure 11

Fitting results of Langmuir model (a) and Freundlich model (b) of TC

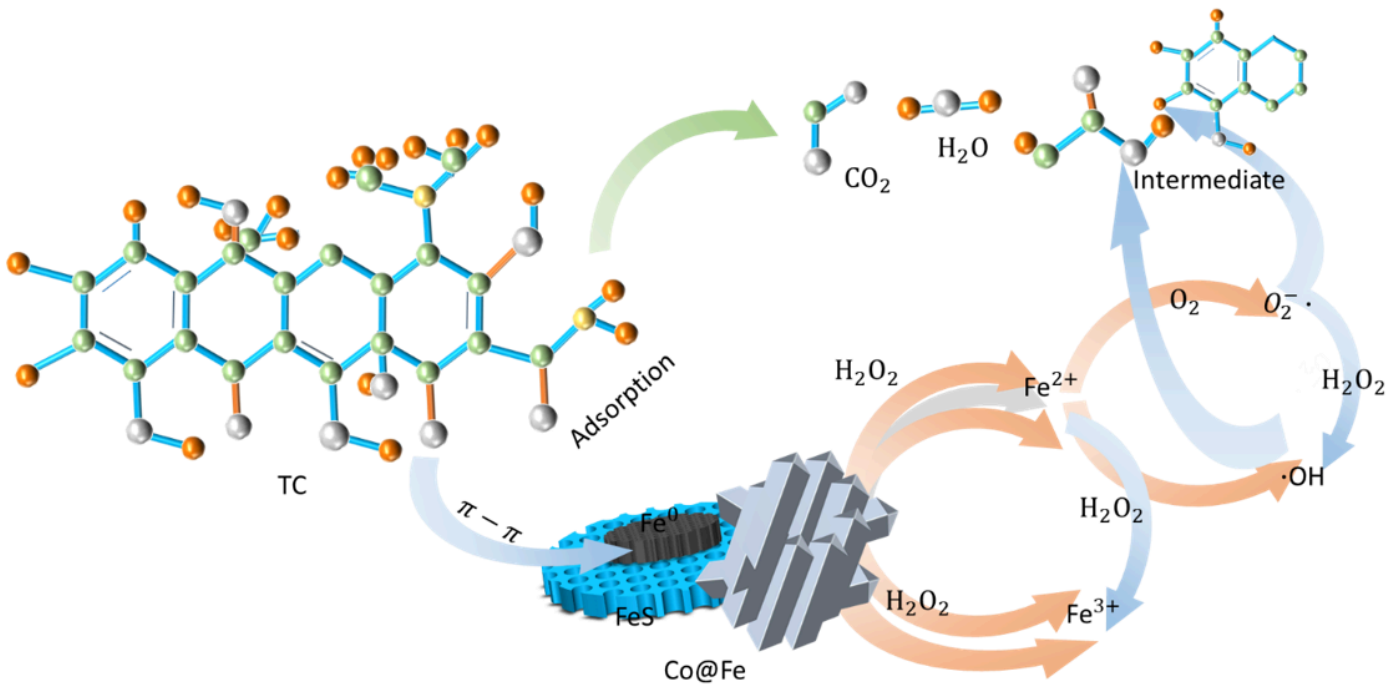


Figure 12

Proposed a mechanism diagram for the adsorption and reduction of TC by nCo@nZVI

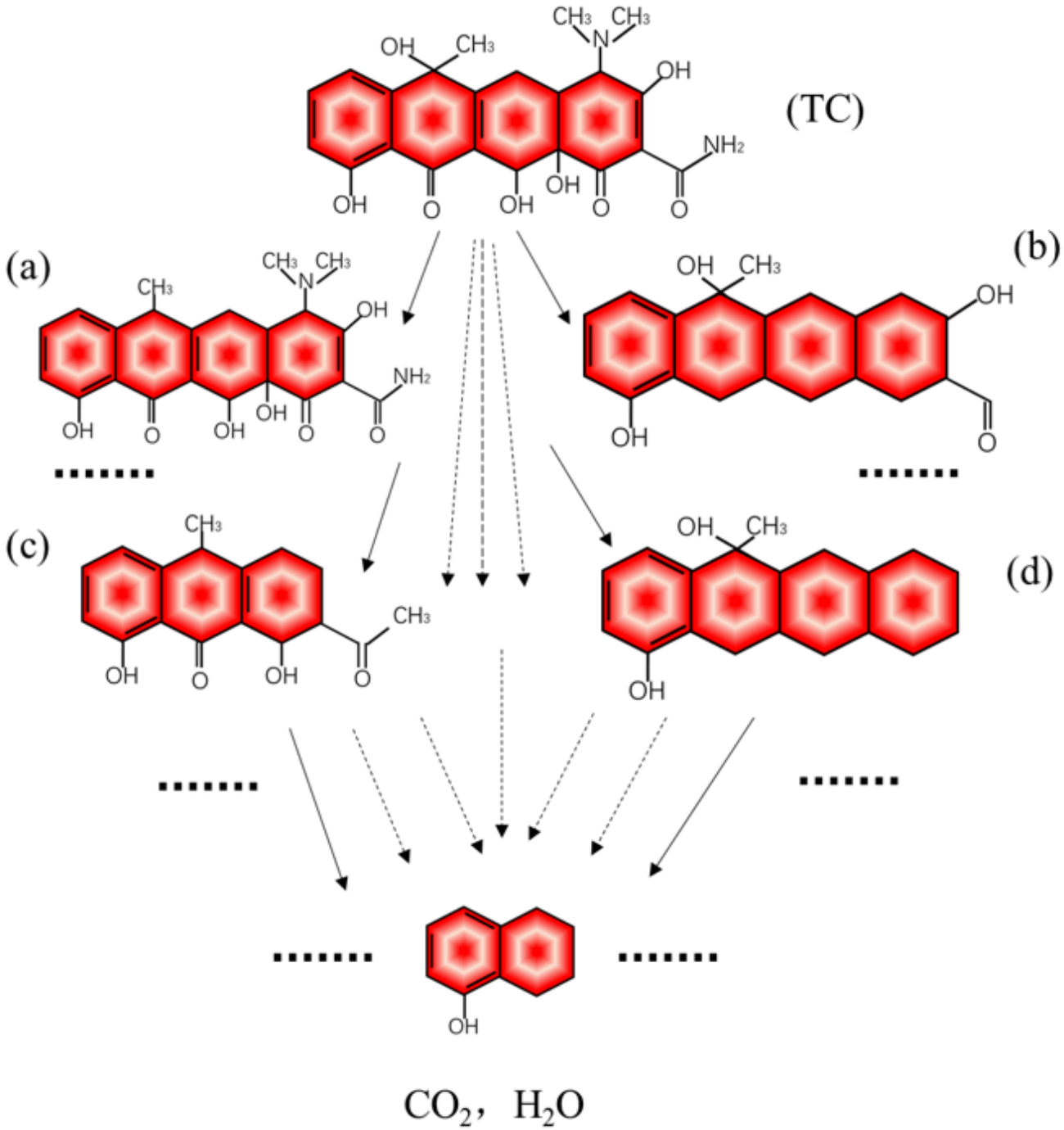


Figure 13

Possible Degradation Pathways of nCo@nZVI During the TC Removal Process

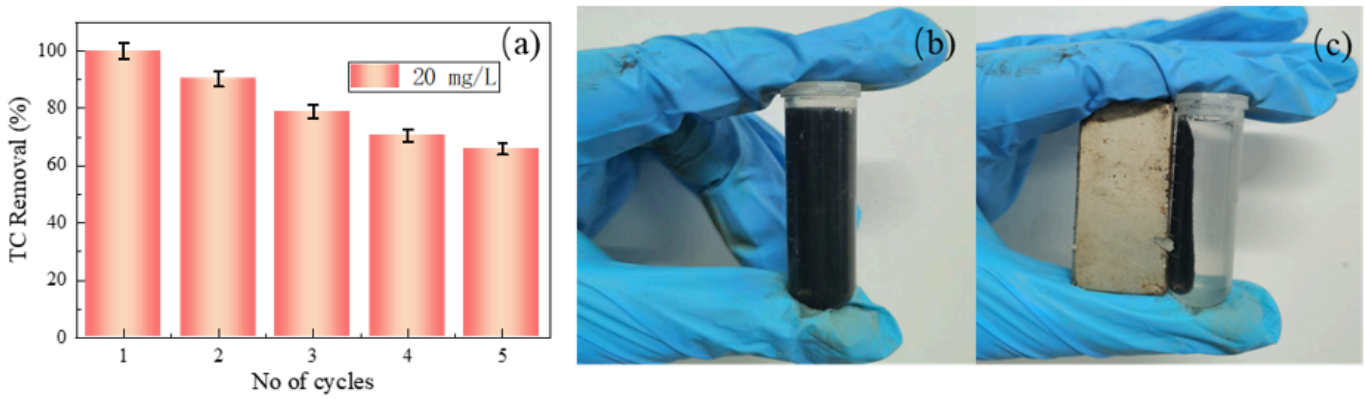


Figure 14

Number of Cycles and Removal Rate of nCo@nZVI (a), magnetic separation (b) and (c) in TC solution